Alisi et al. Beni-Suef University Journal of Basic and Applied Sciences (2019) 8:11
https://doi.org/10.1186/s43088-019-0011-2

Beni-Suef University Journal of Basic and Applied Sciences

RESEARCH Open Access

In silico design of hydrazone antioxidants and analysis of their free radical-scavenging mechanism by thermodynamic studies

Ikechukwu Ogadimma Alisi[1*], Adamu Uzairu[2] and Stephen Eyije Abechi[2]

Abstract

Background: Antioxidants are very crucial in maintaining the normal function of body cells, as they scavenge excess free radical in the body. A set of hydrazone antioxidants was designed by in silico screening. The density functional theory (DFT) method was employed to explore the reaction energetics of their free radical-scavenging mechanism. With the aid of the developed quantitative structure-activity relationship (QSAR) model for hydrazone antioxidants, the structure and antioxidant activity of these compounds were predicted. Three potential reaction mechanisms were investigated, namely, hydrogen atom transfer (HAT), single-electron transfer followed by proton transfer (SET-PT) and sequential proton loss electron transfer (SPLET). Bond dissociation enthalpy (BDE), adiabatic ionization potential (AIP), proton dissociation enthalpy (PDE), proton affinity (PA), electron transfer enthalpy (ETE) and Gibbs free energy that characterize the various steps in these mechanisms were calculated in the gas phase.

Results: A total of 25 hydrazone antioxidants were designed, in which the molecule MHD 017 gave the best antioxidant activity. Among the tested molecules, MHD 017 at the 10-OH site gave the best results for the various thermodynamic parameters calculated. The reaction Gibbs free energy results also indicate that this is the most favoured site for free radical scavenge.

Conclusion: The obtained results show that HAT and SPLET mechanisms are the thermodynamically plausible reaction pathways of free radical scavenge by hydrazone antioxidants. The reactivity of these compounds towards the hydroperoxyl radical (HOO·) was greater than that towards the methyl peroxyl radical (CH_3OO·) based on the exergonicity of the calculated reaction Gibbs free energy.

Keywords: Hydrazone, Free radical, Antioxidant, Scavenging mechanism, In silico design

1 Background

The hydrazones are a group of compounds that contain the azomethine linkage. This linkage influences the majority of their reactions and properties [13]. The derivatives of hydrazone have been demonstrated to display diverse biological activities which include α-glucosidase inhibition [33, 41], antibacterial and anti-fungi [4, 14, 16, 32, 34], anticancer [18, 38], anti-tumor [32], anticonvulsant [11], anticholinesterase [20] and antioxidant [3, 7, 12, 15, 19, 23] activities. Recently, hydrazone derivatives have been employed as corrosion inhibitors for mild steel and iron [10, 21]. They have also been shown to possess photoprotective capacities [7].

The various metabolic processes that take place in the human system result in the production of free radicals which includes reactive oxygen species (ROS). Excessive and uncontrolled production of reactive oxygen species in the human system is the major cause of various disease conditions such as atherosclerosis, cancer, cardiovascular disorders and oxidative damage to proteins and DNA [3, 19]. This condition could be prevented by the application of antioxidant therapeutic agents such as hydrazone derivatives with potent antioxidant activities. Antioxidants are able to interact with free radicals and

* Correspondence: ikeogadialisi@gmail.com; ialisi@fudutsinma.edu.ng
[1]Department of Applied Chemistry, Federal University Dutsinma, PMB 5001, Dutsinma, Katsina State, Nigeria
Full list of author information is available at the end of the article

terminate the chain reactions that cause their damaging effects in the body.

Virtual screening employs computer-based methods in the design and identification of new chemical entities on the basis of their biological activities. Upon the application of virtual screening, a large collection of compounds can be analysed, and candidates with the best potency subjected to synthesis. The key advantages associated with virtual screening are its ability to control cost, time and wastage encountered when screening a large collection of compounds for a particular biological activity. Two broad categories of virtual screening have been distinguished, namely, docking and ligand-based virtual screening [43]. Docking is a structure-based screening method, while ligand-based virtual screening involves the use of active compounds as templates. The particular chosen screening method depends on the information available for the system. Ligand-based approaches employ pharmacophore or quantitative structure-activity relationship quantitative structure-activity relationship (QSAR) models to screen a broad range of ligands [24, 35].

The use of mathematical models such as those generated from QSAR studies, for screening new chemical compounds through the technique of ligand-based virtual screening is gaining popularity in the development of novel compounds with improved biological activities [5, 6, 26]. This research entails a systematic investigation of the free radical-scavenging mechanisms of newly designed hydrazone derivatives by thermodynamic studies. The earlier developed QSAR model for hydrazones [1] was employed in the design of a new set of hydrazone derivatives by ligand-based virtual screening. The antioxidant activities and applicability domain of these compounds were investigated with the aid of the model. The three basic mechanisms of free radical scavenge, namely, hydrogen atom transfer (HAT), single-electron transfer followed by proton transfer (SET-PT) and sequential proton loss electron transfer (SPLET), were investigated for the designed compounds with best antioxidant potentials via thermodynamic studies. This was accomplished by calculating the various antioxidant parameters such as bond dissociation enthalpy (BDE), adiabatic ionization potential (AIP), proton dissociation enthalpy (PDE), proton affinity (PA) and electron transfer enthalpy (ETE). Subsequently, the highest occupied molecular orbital (HOMO) and the lowest unoccupied molecular orbital (LUMO) distributions of the compounds as well as their radical spin density were evaluated. The DFT method has been found to give an accurate evaluation of the above mentioned reaction enthalpies that characterize the various reaction mechanisms. Subsequently, geometry optimization of all molecular structures was conducted in the gas phase at the density functional theory (DFT) level with B3LYP functional and 6-311G* basis set. Also, the thermodynamically preferred mechanism of the reactions between the considered antioxidants and the two important peroxyl radicals (hydroperoxyl radical (HOO·) and methyl peroxyl radical (CH_3OO)) were evaluated through the computation of their reaction Gibbs free energy.

2 Methods

2.1 Ligand-based virtual screening of new compounds

The results of the developed QSAR model for hydrazone antioxidants [1] were employed in the design of a new set of hydrazone compounds by ligand-based virtual screening. The applicability domain for the developed model has a leverage threshold h^*, value of 0.375.

This was performed by insertion, deletion and substitution of different substitutes on the template molecule as dictated by the developed hydrazone antioxidant model [6, 25, 28]. In the present research, compound M010 (Fig. 1) listed in Table 1 of [1], was chosen as a template based on its good antioxidant activity (pIC_{50} = 6.123). The chemical structures of the compounds were drawn using the Chem Draw Program [22]. With the aid of the Spartan 14 program [39], the resulting structures were minimized and further optimized at the density functional theory (DFT) level using the Becke's three-parameter Lee-Yang-Parr hybrid functional (B3LYP) and 6-311G* basis set without symmetry constraints. This resulted in the generation of quantum chemical descriptors. The optimized structures were converted to Sdf files and submitted for the generation of molecular descriptors using the PADEL program package version 2.20 [46]. The effects of the structural modifications on the antioxidant activity of the resulting compounds were investigated. Subsequently, the applicability domain of the newly designed compounds was assessed by the leverage approach.

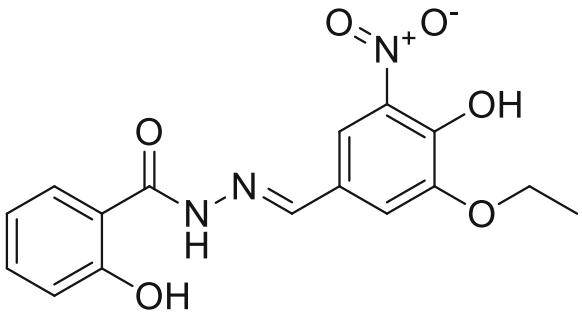

Fig. 1 The parent hydrazone molecule used as a template (M010)

Table 1 Designed hydrazone antioxidants, their predicted antioxidant activities and leverage values

Comp no.	Compound structure/name	plC_{50}	Leverage
MHD 01	(E)-N'-(3-ethoxy-2,4-dihydroxy-5-nitrobenzylidene)-2,5-dihydroxybenzohydrazide	6.470	0.062
MHD 02	(E)-5-amino-N'-(2-amino-3-ethoxy-4-hydroxy-5-nitrobenzylidene)-2-hydroxybenzohydrazide	6.589	0.076
MHD 03	(E)-5-(dichloromethyl)-N'-(2-(dichloromethyl)-3-ethoxy-4-hydroxy-5-nitrobenzylidene)-2-hydroxybenzohydrazide	5.979	0.196
MHD 04	(E)-5-(difluoromethyl)-N'-(2-(difluoromethyl)-3-ethoxy-4-hydroxy-5-nitrobenzylidene)-2-hydroxybenzohydrazide	5.925	0.194
MHD 05	(E)-5-(2,2-dichloroethyl)-N'-(2-(2,2-dichloroethyl)-3-ethoxy-4-hydroxy-5-nitrobenzylidene)-2-hydroxybenzohydrazide	6.424	0.330
MHD 06	(E)-5-(2,2-difluoroethyl)-N'-(2-(2,2-difluoroethyl)-3-ethoxy-4-hydroxy-5-nitrobenzylidene)-2-hydroxybenzohydrazide	6.432	0.398
MHD 07	(E)-N'-(3-ethoxy-4-hydroxy-5-nitrobenzylidene)-2,4,5-trihydroxybenzohydrazide	6.478	0.062
MHD 08	(E)-4,5-diaminoN'-(3-ethoxy-4-hydroxy-5-nitrobenzylidene)-2-hydroxybenzohydrazide	6.575	0.073
MHD 09	(E)-4,5-bis (dichloromethyl)-N'-(3-ethoxy-4-hydroxy-5-nitrobenzylidene)-2-hydroxybenzohydrazide	5.951	0.179
MHD 10	(E)-4,5-bis (difluoromethyl)-N'-(3-ethoxy-4-hydroxy-5-nitrobenzylidene)-2-hydroxybenzohydrazide	5.972	0.157
MHD 11	(E)-4,5-bis(2,2-dichloroethyl)-N'-(3-ethoxy-4-hydroxy-5-nitrobenzylidene)-2-hydroxybenzohydrazide	6.405	0.323
MHD 12	(E)-3-amino-5-(dichloromethyl)-4-(difluoromethyl)-N'-(3-ethoxy-2,4-dihydroxy-5-nitrobenzylidene)-2,6-dihydroxybenzohydrazide	6.543	0.098
MHD 13	(E)-N'-(3-ethoxy-2,4-dihydroxy-5-nitrobenzylidene)-2,3,4,5,6-pentahydroxybenzohydrazide	6.607	0.253
MHD 14	(E)-2,3,4,5-tetraamino-N'-(2-amino-3-ethoxy-4-hydroxy-5-nitrobenzylidene)-6-hydroxybenzohydrazide	6.573	0.216
MHD 15	(E)-2,3,4,5-tetrakis (difluoromethyl)-N'-(2-(difluoromethyl)-3-ethoxy-4-hydroxy-5-nitrobenzylidene)-6-hydroxybenzohydrazide	4.890	0.664
MHD 16	(E)-4-(2,2-dichloroethyl)-N'-(-3-ethoxy-4-hydroxy-5-nitrobenzylidene)-2,6-dihydroxybenzohydrazide	6.613	0.105
MHD 17	(E)-3,5-diamino-N'-(2-amino-3-ethoxy-4-hydroxy-5-nitrobenzylidene)-2,4,6-trihydroxybenzohydrazide	6.851	0.200
MHD 18	(E)-2-amino-N'-(2-amino-3-ethoxy-4-hydroxy-5-nitrobenzylidene)-3-(dichloromethyl)-5-(difluoromethyl)-4,6-dihydroxybenzohydrazide	6.620	0.102
MHD 19	(E)-N'-(3-ethoxy-2,4-dihydroxy-5-nitrobenzylidene)-2,4,6-trihydroxybenzohydrazide	6.541	0.089
MHD 20	(E)-N'-(3-ethoxy-4-hydroxy-2-mercapto-5-nitrobenzylidene)-2-hydroxy-4,6-dimercaptobenzohydrazide	6.318	0.209
MHD 21	(E)-2,4-diamino-N'-(2-amino-3-ethoxy-4-hydroxy-5-nitrobenzylidene)-6-hydroxybenzohydrazide	6.610	0.076
MHD 22	(E)-N'-(2-amino-3-ethoxy-4-hydroxy-5-nitrobenzylidene)-2,4-dihydroxy-6-mercaptobenzohydrazide	6.783	0.115
MHD 23	(E)-N'-(3-ethoxy-4-hydroxy-5-nitrobenzylidene)-3,4'-dihydroxy-[1,1'-biphenyl]-4-carbohydrazide	5.439	0.069
MHD 24	(E)-N'-((6-ethoxy-4',5-dihydroxy-4-nitro-[1,1'-biphenyl]-2-yl)methylene)-3,4'-dihydroxy-[1,1'-biphenyl]-4-carbohydrazide	4.896	0.377
MHD 25	(E)-N'-(3-ethoxy-4-hydroxy-5-nitrobenzylidene)-4,4'',5'-trihydroxy-[1,1'3',1''-terphenyl]-4'-carbohydrazide	4.904	0.378

2.2 Calculation of antioxidant parameters

In order to evaluate the preferred mechanism of free radical scavenge, various antioxidant descriptors were calculated as presented below:

The homolytic bond dissociation enthalpy (BDE): This is the standard enthalpy change at a given temperature when a particular chemical bond is broken under standard conditions [37]. The stability of the corresponding hydroxyl group is determined by the value of the BDE. When the BDE value is low, the stability of the corresponding O–H bond is low and thus can easily be broken (Fuyu and Ruifa 2013). This gives rise to high antioxidant capacity for the considered compound. This parameter was calculated under standard conditions of 1 atm and 298.15 K as presented in Eq. 1.

$$\mathrm{BDE} = H_{\mathrm{radical}} + H_{\mathrm{H}} - H_{\mathrm{neutral}} \quad (1)$$

The adiabatic ionization potential (AIP): This potential describes the process of electron donation by the antioxidant. It represents the capacity of the antioxidant to transfer electrons to the free radical. The lower the AIP value for a given molecule, the easier is the capacity to transfer electrons and the higher the susceptibility of that molecule to undergo ionization. Molecules with high to low AIP values have been observed to possess very strong antioxidant properties.

This parameter was estimated according to Eq. 2;

$$AIP = H_{\text{cation radical}} + H_{\text{electron}} - H_{\text{neutral}} \quad (2)$$

The proton dissociation enthalpy (PDE): This was also calculated using Eq. 3. PDE is a useful physical parameter that describes the ability of the compounds to donate a proton. Antioxidants with lower values of PDE have been observed to be more susceptible to proton abstraction [27].

$$\mathrm{PDE} = H_{\mathrm{radical}} + H_{\mathrm{H^+}} - H_{\text{cation radical}} \quad (3)$$

The proton affinity (PA): This may be defined as the negative of the molar enthalpy change at 298.15 K. The lower the PA value, the higher the antioxidant activity.

This parameter was computed using Eq. (4)

$$\mathrm{PA} = H_{\mathrm{anion}} + H_{\mathrm{H^+}} - H_{\mathrm{neutral}} \quad (4)$$

The electron transfer enthalpy (ETE): Eq. 5 was employed in the calculation of ETE. The lower the ETE value, the more active is the resulting phenoxide anion for a given molecule.

$$\mathrm{ETE} = H_{\mathrm{radical}} + H_{\mathrm{electron}} - H_{\mathrm{anion}} \quad (5)$$

where

H_{radical}= Total enthalpy of phenoxyl radical.
H_{H}= Total enthalpy of the hydrogen atom.
H_{neutral}= Total enthalpy of neutral compound.
$H_{\mathrm{H^+}}$ = Total enthalpy of the proton.
$H_{\mathrm{cation\ radical}}$= Total enthalpy of the cation radical.
H_{electron}= Total enthalpy of the electron.
H_{anion}= Total enthalpy of the anion.

In this research, the total enthalpies of the species were calculated as the sum of total electronic energy, zero-point energy and the translational, rotational and vibrational contributions to the total enthalpy (Eq. 6). The RT (PV-work) term was added to convert the energy to enthalpy [29].

$$H = E_0 + \mathrm{ZPE} + H_{\mathrm{trans}} + H_{\mathrm{rot}} + H_{\mathrm{vib}} + \mathrm{RT} \quad (6)$$

where, H_{trans}, H_{rot} and H_{vib} are the translational, rotational, and vibrational contributions to the enthalpy, respectively. E_0 is the total energy at 0 K, while ZPE is the zero-point vibrational energy.

Also, for the calculation of the antioxidant parameters, the following values were employed: $H(H^{\bullet})_{\mathrm{vacuum}}$=−1312.479673 kJ/mol, $H(H^{+})_{\mathrm{vacuum}}$= 6.1961805 kJ/mol, and $H(e^{-})_{\mathrm{vacuum}}$= 3.14534924 kJ/mol, [8, 9, 30, 36].

2.3 Investigation of the thermodynamically favoured mechanism

The thermodynamically favoured mechanism is estimated by the reaction Gibbs free energy ($\Delta_r G$) [2, 47]. In this light, computation of the Gibbs free energy of the reactants and products for the studied mechanisms of the reactions between the antioxidants and the two important peroxyl radicals (HOO· and CH_3 – OO·) were performed.

The reaction between a free radical and an antioxidant is said to be thermodynamically favourable if the reaction Gibbs free energy is negative (Eq. 7).

$$\Delta_r G = [G(\mathrm{products}) - G(\mathrm{reactants})] < 0 \quad (7)$$

The reaction Gibbs free energy for the HAT mechanism is given by $\Delta_r G_{\mathrm{BDE}}$. This was calculated as presented in Eq. 8.

$$\Delta_r G_{\mathrm{BDE}} = [G(H_{n-1}\mathrm{Antiox}^{\bullet}) + G(RH)] - [G(H_n\mathrm{Antiox}) + G(R^{\bullet})] \quad (8)$$

The reaction Gibbs free energy for the SET-PT mechanism is given by $\Delta_r G_{\mathrm{AIP}}$ (Eq. 9) and $\Delta_r G_{\mathrm{PDE}}$ (Eq. 10).

$$\Delta_r G_{\mathrm{AIP}} = [G(H_{n-1}\mathrm{Antiox}^{\bullet+}) + G(R^{-})] - [G(H_n\mathrm{Antiox}) + G(R^{\bullet})] \quad (9)$$

$$\Delta_r G_{\mathrm{PDE}} = [G(H_{n-1}\mathrm{Antiox}^{\bullet}) + G(RH)] - [G(H_{n-1}\mathrm{Antiox}^{\bullet+}) + G(R^{-})] \quad (10)$$

Also, the reaction Gibbs free energy for the SPLET mechanism is given by $\Delta_r G_{\mathrm{PA}}$ (Eq. 11) and $\Delta_r G_{\mathrm{ETE}}$ (Eq. 12).

$$\Delta_r G_{\mathrm{PA}} = [G(H_{n-1}\mathrm{Antiox}^{-}) + G(RH)] - [G(H_n\mathrm{Antiox}) + G(R^{-})] \quad (11)$$

$$\Delta_r G_{\mathrm{ETE}} = [G(H_{n-1}\mathrm{Antiox}^{\bullet}) + G(R^{-})] - [G(H_{n-1}\mathrm{Antiox}^{-}) + G(R^{\bullet})] \quad (12)$$

where

$G(H_n Antiox)$ = Gibbs free energy of neutral antioxidant.
$G(H_{n-1}\mathrm{Antiox}^{\bullet})$ = Gibbs free energy of phenoxyl radical.
$G(R^{\bullet})$ = Gibbs free energy of free radical.
$G(RH)$ = Gibbs free energy of product formed by hydrogen abstraction to free radical.
$G(H_{n-1}\mathrm{Antiox}^{\bullet+})$ = Gibbs free energy of cation radical.
$G(H^{+})$ = Gibbs free energy of proton.
$G(R^{-})$ = Gibbs free energy of free radical anion.
$G(H_{n-1}\mathrm{Antiox}^{-})$ = Gibbs free energy of anion.

In the above calculations, the values of −3.72 kJ/mol and −26.28 kJ/mol were employed as the Gibbs free energy of the electron (e^{-}) and proton (H^{+}) respectively [17, 42].

3 Results

4 Discussions

4.1 Virtual screening results

The predicted activities and leverage values of the designed hydrazone antioxidants are presented in Table 1. The applicability domain of the hydrazone model has a leverage threshold, h^{*} value of 0.375. All the developed molecules were found within the applicability domain of the model except MHD 06, MHD 15, MHD 24, and MHD 25. Also, majority of the molecules have improved antioxidant activities compared to MHD 10 with MHD 17, MHD 21 and MHD 22 having the best pIC_{50} values of 6.851, 6.610 and 6.783, respectively. These molecules were subsequently selected and subjected to quantum

chemical calculations in order to investigate their preferred mechanism of free radical scavenge. The molecular structure and carbon atom numbering for these three compounds are presented in Fig. 2.

4.2 Analysis of the HAT mechanism

The computed BDE results for MHD 017, MHD 021 and MHD 022 are presented in Table 2. For MHD 017, the 8-NH position has the highest BDE value of 379.156 kJ/mol. This is closely followed by the 14-OH position with a value of 373.984 kJ/mol. These high values of BDE could be attributed to the tendency of the hydrogen atoms at these positions to form intramolecular hydrogen bonds with the adjacent carbonyl group of the parent molecule. For this reason, hydrogen atom abstraction is more difficult at these positions in comparison to the other positions. Also, HAT occurs more easily at the 10-OH position since it has the lowest BDE value of 255.968 kJ/mol. A similar trend is observed for MHD 021 where the 14-NH position has the highest BDE value of 387.742 kJ/mol due to the possible formation of an intramolecular hydrogen bond with the adjacent ketone group of the parent molecule. While the 10-OH position has the lowest BDE value of 296.506 kJ/mol. Therefore HAT occurs more readily at this position. An examination of the BDE results of MHD 022 reveals that apart from the 10-OH and 14-SH positions which have lower BDE values of 305.800 kJ/mol and 307.060 kJ/mol, the 2-OH, 4-NH, 8-NH and 12-OH positions have very close and higher BDE results of 348.097 kJ/mol, 356.551 kJ/mol, 365.609 kJ/mol and 341.244 kJ/mol, respectively. Based on this result, the preferred site of free radical scavenge for MHD 022 is the 10-OH and 14-SH positions. The lower BDE value of MHD 022 14-SH against the higher values observed for MHD 017 14-OH and MHD 021 14-NH could be attributed to the less electronegative nature of sulphur in comparison to oxygen or nitrogen which form stronger intramolecular hydrogen bonds with the adjacent carbonyl group of the parent molecule. From the ongoing discussions, we observe that for MHD 017, MHD 021 and MHD 022 the lowest values of BDE occurred at the 10-OH positions on the A ring for each of the molecules with values of 255.968 kJ/mol, 296.506 kJ/mol and 305.800 kJ/mol. These results are by far lower than the BDE of phenol (327.550 kJ/mol) at the same level of theory, which is generally chosen as the reference compound. This implies that the –OH group at this position is the possible set of free radical scavenge and contributes mainly to the antioxidant activities of hydrazone derivatives through the HAT mechanism. While the –OH and –NH groups at other positions in these molecules have relatively little influence on the HAT mechanism.

4.3 Analysis of the spin density distribution

Apart from the magnitude of the BDE, another important factor that influences the antioxidant activity of phenolic antioxidants is the stability of the radical. The radical spin density distribution is very useful in rationalizing the stability of a given radical species [44, 45, 47]. The spin density results on the radicals of MHD 017, MHD 021 and MHD 022 are also presented in Table 2. For a given radical, the lower the spin density, the higher the delocalisation of the spin density in the radical, the easier the radical is formed, the lower the BDE. For instance, among the MHD 017, MHD 021 and MHD 022 molecule, the 10-OH radicals for each of the considered compounds have the lowest spin density values of 0.000121, 0.000181 and 0.000219, respectively. These positions also possess the lowest BDE values (Table 2). Based on these results, the radicals produced at the 10-OH position for each of these antioxidants are the most stable. This position also represents the most favoured site for free radical attack based on the HAT mechanism.

4.4 Analysis of SET-PT mechanism

The adiabatic ionization potential (AIP) and proton dissociation enthalpy (PDE) values for MHD 017, MHD 021 and MHD 022 molecules and their radicals were calculated and presented in Table 2. The first step of SET-PT mechanism is characterized by AIP. Apart from MHD 022 12-OH with an AIP value of 595.379 kJ/mol, the other scavenging sites of the considered molecules

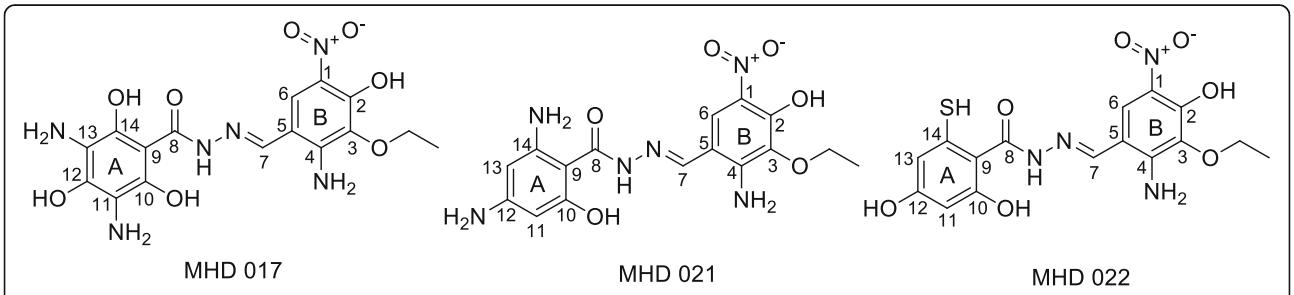

Fig. 2 Molecular structure and carbon atom numbering of MHD 017, MHD 021 and MHD 022

Table 2 Antioxidant properties of designed hydrazone derivatives calculated at the B3LYP/6-311G* level in a vacuum

Comp no.	HAT	SET-PT		SPLET		Spin density
	BDE (KJ/mol)	AIP (KJ/mol)	PDE (KJ/mol)	PA (KJ/mol)	ETE (KJ/mol)	
MHD 017 2-OH	347.755	432.835	1236.742	1388.443	281.133	0.000225
MHD 017 4-NH	357.260	438.453	1240.628	1396.924	282.157	0.000573
MHD 017 8-NH	379.156	449.900	1251.077	1406.743	294.235	0.000255
MHD 017 10-OH	255.968	385.996	1191.793	1352.553	225.236	0.000121
MHD 017 11-NH	318.376	424.591	1215.607	1352.500	287.697	0.000583
MHD 017 12-OH	278.180	397.837	1202.164	1375.683	224.317	0.000123
MHD 017 13-NH	321.422	397.863	1245.38	1535.419	107.824	0.000604
MHD 017 14-OH	373.984	379.878	1315.927	1398.026	297.779	0.000217
MHD 021 2-OH	343.686	417.659	1247.848	1403.487	262.020	0.000217
MHD 021 4-NH	354.293	423.278	1252.836	1410.734	265.380	0.000553
MHD 021 8-NH	368.576	378.356	1312.041	1413.333	277.064	0.000396
MHD 021 10-OH	296.506	354.464	1263.863	1347.354	270.973	0.000181
MHD 021 12-NH	370.886	442.418	1250.289	1464.583	228.124	0.000717
MHD 021 14-NH	387.742	342.517	1367.045	1519.167	190.396	0.000746
MHD 022 2-OH	348.097	436.510	1233.407	1383.323	286.594	0.000222
MHD 022 4-NH	356.551	443.468	1234.904	1414.436	263.936	0.000571
MHD 022 8-NH	365.609	421.571	1265.859	1368.043	319.387	0.000382
MHD 022 10-OH	305.800	386.022	1241.599	1305.635	321.986	0.000219
MHD 022 12-OH	341.244	595.379	1067.686	1355.966	307.100	0.000316
MHD 022 14-SH	307.060	384.184	1244.697	1276.256	352.626	0.001080
Phenol	327.550	572.776	1076.594	1462.892	186.479	

have AIP values well below that of phenol (572.776 kJ/mol at the same level of theory), which is chosen as our reference molecule (Table 2). This is an indication that the electron-donating ability of these molecules at the various considered sites is stronger than that of phenol. Also, the trend of the AIP results is significantly different from those of BDE for the considered molecules. This discrepancy could be attributed to the fact that BDE is influenced by local phenomena resulting from the various substituents in the molecule, whereas AIP results are influenced by the structure of the entire molecule (extended delocalization and conjugation of the π-electrons) [44, 45]. For MHD 017, MHD 021 and MHD 022 the lowest value of AIP is found for MHD 017 14-OH (379.878 kJ/mol), MHD 021 14-NH (342.517 kJ/mol) and MHD 022 14-SH (384.184 kJ/mol), respectively. For each of these molecules, these sites possess stronger electron-donating ability in comparison to the other sites.

The PDE characterizes the second step of the SET-PT mechanism. For each of the molecules MHD 017, MHD 021 and MHD 022, the highest values of PDE occurred at the 8-NH, 14-NH and 8-NH positions, respectively. This trend is analogous to those of BDE where these sites also record the highest values. This could be attributed to the fact that the second step of the SET-PT mechanism results in the generation of free radicals as in the HAT mechanism.

From the thermodynamic point, the first step is the most important for reactions that involve multiple-step mechanisms. Consequently, the results of AIP determine the order and magnitude in which these molecules undergo the SET-PT mechanism.

4.5 Analysis of SPLET mechanism

The proton affinity (PA) and electron transfer enthalpy (ETE) values for MHD 017, MHD 021 and MHD 022 hydrazone antioxidant molecules are presented in Table 2. The PA value is the antioxidant parameter that characterizes the first step of SPLET mechanism. The second step is characterized by ETE. For MHD 017, MHD 021 and MHD 022, the lowest observed PA values are 1352.500 kJ/mol, 1347.354 kJ/mol and 1276.256 kJ/mol which occur at the 11-NH, 10-OH and 14-SH positions, respectively. For each of these molecules, these are the most favoured sites for deprotonation to generate highly stabilized anions. PA results at these sites are also more favourable when compared with that of phenol which has a value of 1462.892 kJ/mol.

The ETE results for MHD 017, MHD 021 and MHD 022 recorded lowest values at the 13-NH, 14-NH and 4NH respectively. These are the sites that are most favoured to undergo electron transfer in the second step of the SPLET mechanism in each of the considered molecules. When the ETE results are compared with those of AIP, the ETE values are found to be lower. Accordingly, the single-electron transfer from the neutral form of the hydrazone antioxidant to the free radical is less favourable to that from the anionic form.

4.6 Thermodynamically preferred mechanism

The results of the Gibbs free energy change of reactions of inactivation of HOO· and CH_3OO· via HAT, SET-PT and SPLET mechanisms by MHD 017, MHD 021 and MHD 022 molecules are presented in Tables 3 and 4, respectively. The values of the reaction Gibbs free energy ($\Delta_r G$) are quite helpful in the assignment of the free radical-scavenging potency of molecules, because more negative values indicate the thermodynamically more preferred reactions. The results presented in Table 3 reveal that MHD 017 (at the 10-OH, 11-NH and 12-OH), MHD 021 (at the 10-OH) and MHD 022 (at the 10-OH and 14-SH) sites could scavenge HOO· by HAT and SPLET mechanisms because these processes are exergonic. The results at the other positions are thermodynamically unfavourable due to their endergonic nature. In the SPLET pathway, we observe that the exergonicity of $\Delta_r G_{PA}$ results overwhelm the endergonicity of the $\Delta_r G_{ETE}$ results. Since a thermodynamically unfavourable reaction could be driven by a thermodynamically favourable reaction that is coupled to it, the entire SPLET mechanism is exergonic. A similar result to the HOO· scavenge is observed for the CH_3OO· scavenge except for the 11-NH position of MHD 017 molecule where the reaction is endergonic (Table 4). On the basis of the exergonicity of the calculated reaction Gibbs free energy for each considered hydrazone antioxidant molecule, the 10-OH position appears to be the most efficient site for the scavenge of HOO· and CH_3OO· in the studied environment via HAT and SPLET mechanisms. The Gibbs free energy of these reactions also indicates that these molecules are more efficient in scavenging HOO· than CH_3OO·. On the basis of the calculated reaction free energies, MHD 017 at the 10-OH site possessed the highest free radical-scavenging potency for HOO· than CH_3OO· via HAT and SPLET mechanisms. Subsequently, the radical-scavenging mechanism of this

Table 3 The reaction Gibbs free energy ($\Delta_r G$ in kJ/mol) of scavenging HOO· radical by hydrazone antioxidants at the B3LYP/6-311G* level in a vacuum

Comp no.	HAT	SET-PT		SPLET	
	$\Delta_r G_{BDE}$	$\Delta_r G_{AIP}$	$\Delta_r G_{PDE}$	$\Delta_r G_{PA}$	$\Delta_r G_{ETE}$
MHD 017 2-OH	24.580	562.647	− 538.067	− 248.081	272.661
MHD 017 4-NH	36.158	568.870	− 532.711	− 238.130	274.289
MHD 017 8-NH	56.217	580.159	− 523.942	− 227.655	283.872
MHD 017 10-OH	− 66.310	515.782	− 582.097	− 283.683	217.368
MHD 017 11-NH	− 2.200	554.351	− 556.551	− 283.735	281.535
MHD 017 12-OH	− 43.340	527.702	− 571.044	− 260.473	217.132
MHD 017 13-NH	1.4492	527.754	− 526.305	− 101.447	102.896
MHD 017 14-OH	49.286	510.584	− 461.298	− 237.894	287.180
MHD 021 2-OH	20.353	547.104	− 526.751	− 232.538	252.891
MHD 021 4-NH	33.034	553.484	− 520.450	− 223.506	256.540
MHD 021 8-NH	45.636	509.612	− 463.976	− 219.699	265.336
MHD 021 10-OH	− 24.410	486.298	− 510.710	− 285.652	261.240
MHD 021 12-NH	51.255	573.701	− 522.446	− 168.686	219.941
MHD 021 14-NH	67.166	474.378	− 407.213	− 115.204	182.370
MHD 022 2-OH	25.105	566.586	− 541.481	− 252.728	277.833
MHD 022 4-NH	36.027	574.173	− 538.146	− 243.591	279.618
MHD 022 8-NH	42.696	552.749	− 510.053	− 265.436	308.131
MHD 022 10-OH	− 14.650	516.806	− 531.451	− 327.765	313.120
MHD 022 12-OH	19.775	724.352	− 704.577	− 278.458	298.233
MHD 022 14-SH	− 13.910	515.677	− 529.587	− 356.068	342.158

Table 4 The reaction Gibbs free energy ($\Delta_r G$ in kJ/mol) of scavenging CH_3OO· radical by hydrazone antioxidants at the B3LYP/6-311G* level in a vacuum

Comp No	HAT	SET-PT		SPLET	
	$\Delta_r G_{BDE}$	$\Delta_r G_{AIP}$	$\Delta_r G_{PDE}$	$\Delta_r G_{PA}$	$\Delta_r G_{ETE}$
MHD 017 2-OH	27.817	524.625	− 496.808	− 206.821	234.638
MHD 017 4-NH	39.396	530.847	− 491.452	− 196.871	236.266
MHD 017 8-NH	59.454	542.137	− 482.682	− 186.395	245.849
MHD 017 10-OH	− 63.078	477.760	− 540.837	− 242.423	179.345
MHD 017 11-NH	1.0371	516.328	− 515.291	− 242.475	243.513
MHD 017 12-OH	− 40.105	489.679	− 529.784	− 219.214	179.109
MHD 017 13-NH	4.6865	489.732	− 485.045	− 60.187	64.8735
MHD 017 14-OH	52.523	472.561	− 420.038	− 196.634	249.157
MHD 021 2-OH	23.590	509.082	− 485.492	− 191.278	214.868
MHD 021 4-NH	36.271	515.462	− 479.191	− 182.246	218.518
MHD 021 8-NH	48.874	471.590	− 422.716	− 178.439	227.313
MHD 021 10-OH	− 21.175	448.275	− 469.450	− 244.392	223.217
MHD 021 12-NH	54.492	535.678	− 481.186	− 127.426	181.918
MHD 021 14-NH	70.403	436.356	− 365.953	− 73.9446	144.347
MHD 022 2-OH	28.342	528.563	− 500.221	− 211.468	239.811
MHD 022 4-NH	39.264	536.151	− 496.886	− 202.332	241.596
MHD 022 8-NH	45.933	514.727	− 468.793	− 224.176	270.109
MHD 022 10-OH	− 11.408	478.784	− 490.191	− 286.505	275.097
MHD 022 12-OH	23.012	686.329	− 663.317	− 237.198	260.211
MHD 022 14-SH	− 10.673	477.655	− 488.327	− 314.808	304.135

molecule by HAT and SPLET mechanisms are presented in Scheme 1(a) and (b) respectively.

4.7 Analysis of frontier molecular orbitals

The results of frontier orbital distribution and energy for MHDM 017, MHDM 021 and MHDM 022 calculated at the B3LYP/6-311G* level in the gas phase are presented in Fig. 3. From Fig. 3, we observe that the LUMO is localized on ring B and its associated oxygen and nitrogen atoms in its functional groups for the three molecules. While the HOMO is delocalised almost over the entire molecules, they are observed to be highly concentrated on the nitrogen atoms of the hydrazine group. For MHDM 022, this includes the sulphur atom to which the hydrogen atom is attached. For MHDM 021, this includes the conjugated carbon atoms of ring A, and the nitrogen atom of the amino group. In all the molecules, they are equally distributed on the oxygen atoms of the hydroxyl groups. These sites with a high concentration of the HOMO possess higher tendency to lose electrons [31, 40, 44, 45]. These are the sites for free radical scavenge for the associated molecules.

MHDM 021 has the highest HOMO value of − 5.50 eV, followed by MHDM 017 with a value of − 5.94 eV. This is closely followed by MHDM 022 with a value of − 6.00 eV. Based on this result, MHD 021 has the greatest capacity to lose electrons, because the higher the HOMO energy, the easier the electron is excited. While MHDM 022 has the weakest electron-donating ability among the considered molecules, the sequence of predicted electron-donating ability of these molecules as predicted by the HOMO energies is in very good agreement with that of the predicted AIP results (Table 2).

5 Conclusion

In this research, virtual screening by the method of quantitative structure-activity relationship was employed in the design of new hydrazone antioxidants with the earlier proposed antioxidant model for hydrazones. The structure and antioxidant activity of these compounds were successfully predicted in this work with (E)-3,5-diamino-N'-(2-amino-3-ethoxy-4-hydroxy-5-nitrobenzylidene)-2,4,6-trihydroxybenzohydrazone (MHD 017) having the best antioxidant activity (pIC_{50} = 6.851). This demonstrates the ability of the developed hydrazone antioxidant model to reduce the time and cost of synthesizing new hydrazone antioxidants in addition to the investigation of their antioxidant activities.

The thermodynamics of three of the best antioxidants (MHD 017, MHD 021 and MHD 022) were investigated by the DFT method in the gas phase. In order to evaluate the possible mechanism of free radical scavenge by these molecules, thermodynamic parameters such as BDE, PDE, AIP, PA and ETE were calculated. The radical spin density was also calculated in order to rationalize the observed differences in the BDE results. The sequence of hydrogen donation by these molecules is MHD 017 > MHD 022 > MHD 021 and is in line with their predicted antioxidant activities. The trend of the BDE results is significantly different from those of the AIP, but analogous to those of PDE. Also, from the generated results for AIP and ETE, the single-electron transfer from the neutral form of the hydrazone antioxidant to the free radical is less favourable to that from the anionic form.

The thermodynamically preferred mechanism of reaction was investigated by calculating the reaction Gibbs free energy for inactivating HOO· and CH_3OO· at the various reaction sites in each molecule. The observed results indicate that HAT and SPLET mechanisms are thermodynamically

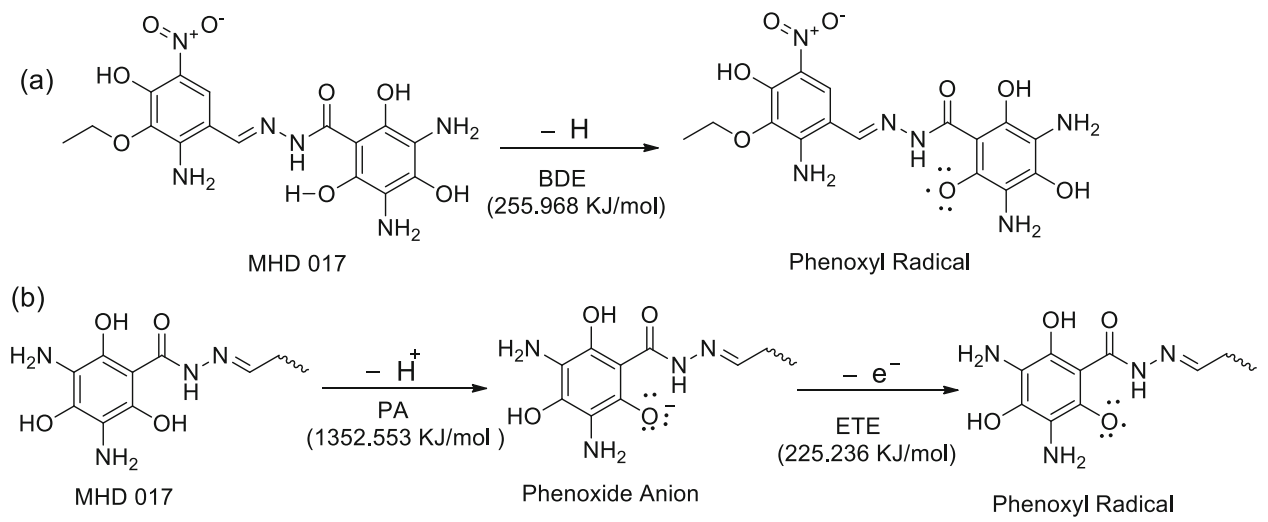

Scheme 1 **a** HAT mechanism of MHD 017 in vacuum. **b** SPLET mechanism of MHD 017 in vacuum

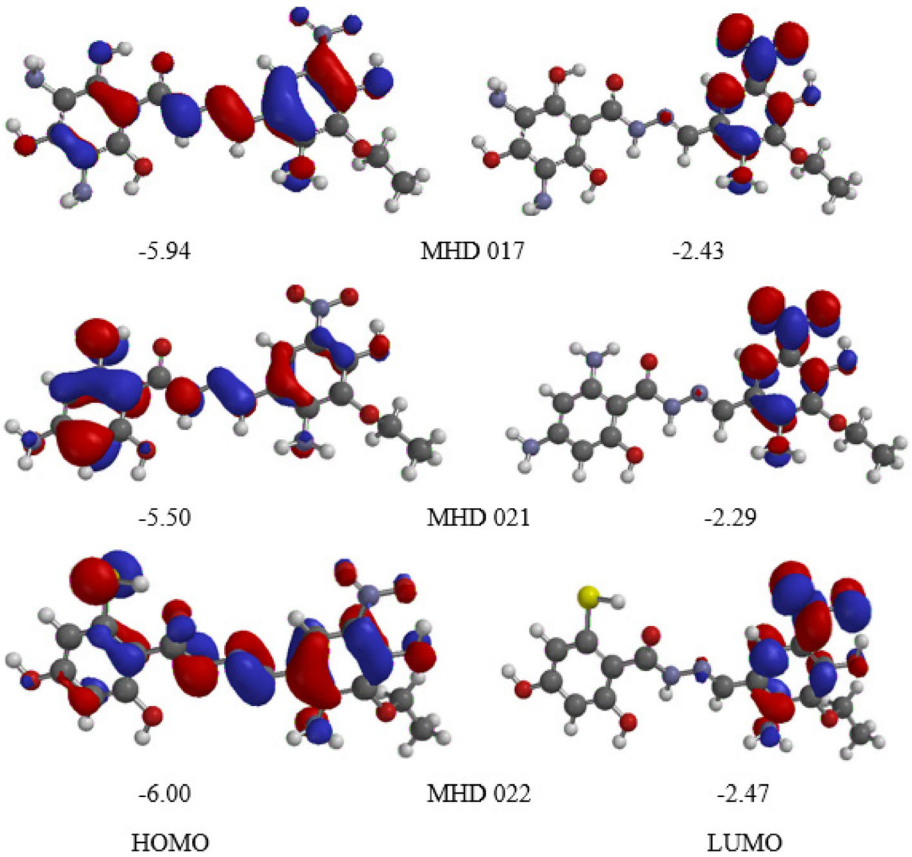

Fig. 3 The orbital distribution and energy (in eV) of HOMO and LUMO for MHD 017, MHD 021 and MHD 022 computed at the B3LYP/6-311G* level in the gas phase

feasible at various sites in each molecule with best results observed at the 10-OH site based on the negative values of their reaction Gibbs free energy. On the other hand, the SET-PT mechanism was thermodynamically unfeasible for all the molecules as their reaction processes were endergonic. Among the tested molecules, MHD 017 which was earlier proposed to have the best antioxidant activity exhibited the highest free radical-scavenging potential against HOO· than CH_3OO· at the 10-OH site upon thermodynamic studies. The present research not only did succeed in the elucidation of the free radical-scavenging mechanism of the considered hydrazone derivatives, but also will stimulate subsequent exploitation of these compounds in the field of food chemistry and pharmacy.

Abbreviations

AIP: Adiabatic ionization potential; B3LYP: Becke's three-parameter Lee-Yang-Parr hybrid functional; BDE: Bond dissociation enthalpy; DFT: Density functional theory; ETE: Electron transfer enthalpy; HAT: Hydrogen atom transfer; HOMO: Highest occupied molecular orbital; LUMO: Lowest unoccupied molecular orbital; PA: Proton affinity; PDE: Proton dissociation enthalpy; QSAR: Quantitative structure-activity relationship; ROS: Reactive oxygen species; SET-PT: Single-electron transfer followed by proton transfer; SPLET: Sequential proton loss electron transfer

Acknowledgements

The authors are grateful to the Physical Chemistry team in Ahmadu Bello University Zaria and Federal University Dutsinma for their assistance.

Authors' contributions

This research was designed by IOA, AU, and SEA. IOA optimized all the molecular structures. All authors participated in the calculation of the thermodynamic parameters. IOA wrote the manuscript under the supervision of AU and SEA. All authors read and approved the final manuscript.

Funding

Not applicable

Availability of data and materials

All data generated or analysed during this study are included in this published article.

Ethics approval and consent to participate

Not applicable

Consent for publication

Not applicable

Competing interests

The authors declare that they have no competing interests.

Author details

[1]Department of Applied Chemistry, Federal University Dutsinma, PMB 5001, Dutsinma, Katsina State, Nigeria. [2]Department of Chemistry, Ahmadu Bello University, Zaria, Kaduna State, Nigeria.

Received: 6 July 2019 Accepted: 6 September 2019
Published online: 28 October 2019

References

1. Alisi IO, Uzairu A, Abechi SE, Idris SO (2018) Free radical scavenging activity evaluation of hydrazones by quantitative structure activity relationship. J Mex Chem Soc 62(1):1–13. https://doi.org/10.29356/jmcs.v62i1.585
2. Amic A, Lučić B, Stepanić V, Marković Z, Marković S, Dimitrić Marković J, Amić D (2017) Free radical scavenging potency of quercetin catecholic colonic metabolites: thermodynamics of 2H+/2e- processes. Food Chem 218:144–151. https://doi.org/10.1016/j.foochem.2016.09.018
3. Anastassova NO, Yancheva DY, Mavrova AT, Kondeva-Burdina MS, Tzankova VI, Hristova-Avakumova NG, Hadjimitova VA (2018) Design, synthesis, antioxidant properties and mechanism of action of new N,N′-disubstituted benzimidazole-2-thione hydrazone derivatives. J Mol Struct 1165:162–176. https://doi.org/10.1016/j.molstruc.2018.03.119
4. Aradhyula BPR, Joshi N, Poluri KM, Kollipara MR (2018) Synthesis and antibacterial studies of rhodium and iridium complexes comprising of dipyridyl hydrazones. J Mol Struct 1164:191–199. https://doi.org/10.1016/j.molstruc.2018.03.058
5. Arthur DE, Uzairu A, Mamza P, Abechi SE, Shallangwa G (2018) In silico modelling of quantitative structure–activity relationship of multi-target anticancer compounds on k-562 cell line. Netw Model Anal Health Inform Bioinform 7(1). https://doi.org/10.1007/s13721-018-0168-y
6. Asadollahi T, Dadfarnia S, Shabani AMH, Ghasemi JB, Sarkhosh M (2011) QSAR models for CXCR2 receptor antagonists based on the genetic algorithm for data preprocessing prior to application of the pls linear regression method and design of the new compounds using in silico virtual screening. Molecules 16:1928–1955. https://doi.org/10.3390/molecules16031928
7. Baldisserotto A, Demurtas M, Lampronti I, Moi D, Balboni G, Vertuani S et al (2018) Benzofuran hydrazones as potential scaffold in the development of multifunctional drugs: synthesis and evaluation of antioxidant, photoprotective and antiproliferative activity. Eur J Med Chem 156:118–125. https://doi.org/10.1016/j.ejmech.2018.07.001
8. Bartmess JE (1994) Thermodynamics of the electron and the proton. J Phys Chem 98:6420–6424. https://doi.org/10.1021/j100076a029
9. Bizarro MM, Cabral BJC, Santos RMB, Simoes JAM (1999) Substituent effects on the O–H bond dissociation enthalpies in phenolic compounds: agreements and controversies. Pure Appl Chem 71(7):1249–1256
10. Chafai N, Chafaa S, Benbouguerra K, Hellal A, Mehri M (2019) Synthesis, spectral analysis, anti-corrosive activity and theoretical study of an aromatic hydrazone derivative. J Mol Struct 1181:83–92. https://doi.org/10.1016/j.molstruc.2018.12.073
11. Dehestani L, Ahangar N, Hashemi SM, Irannejad H, Honarchian Masihi P, Shakiba A, Emami S (2018) Design, synthesis, in vivo and in silico evaluation of phenacyl triazole hydrazones as new anticonvulsant agents. Bioorg Chem 78:119–129. https://doi.org/10.1016/j.bioorg.2018.03.001
12. Demurtas M, Baldisserotto A, Lampronti I, Moi D, Balboni G, Pacifico S et al (2019) Indole derivatives as multifunctional drugs: synthesis and evaluation of antioxidant, photoprotective and antiproliferative activity of indole hydrazones. Bioorg Chem 85:568–576. https://doi.org/10.1016/j.bioorg.2019.02.007
13. El-Din NS, Barseem A (2016) Synthesis, bioactivity and docking study of some new indole-hydrazone derivatives. J Appl Pharm Sci 6(12):075–083. https://doi.org/10.7324/JAPS.2016.601211
14. El-Sayed HA, Moustafa AH, Abd El-Moneim M, Awad HM, Esmat A (2018) Design and synthesis of hydrazide-hydrazones based 2-oxonicotinonitrile derivatives as potential antimicrobial agents. J Pharm Appl 4(2):125–131. https://doi.org/10.18576/jpac/040207
15. Emami S, Esmaili Z, Dehghan G, Bahmani M, Hashemi SM, Mirzaei H, Moradi SE (2018) Acetophenone benzoylhydrazones as antioxidant agents: synthesis, in vitro evaluation and structure-activity relationship studies. Food Chem 268:292–299. https://doi.org/10.1016/j.foodchem.2018.06.083
16. He L-Y, Qiu X-Y, Cheng J-Y, Liu S-J, Wu S-M (2018) Synthesis, characterization and crystal structures of vanadium (V) complexes derived from halido-substituted tridentate hydrazone compounds with antimicrobial activity. Polyhedron. 156:105–110. https://doi.org/10.1016/j.poly.2018.09.017
17. Hwang S, Chung DS (2005) Calculation of the solvation free energy of the proton in methanol. Bull Kor Chem Soc 26:589–593
18. Kaplánek R, Havlík M, Dolenský B, Rak J, Džubák P, Konečný P et al (2015) Synthesis and biological activity evaluation of hydrazone derivatives based on a Tröger's base skeleton. Bioorg Med Chem 23(7):1651–1659. https://doi.org/10.1016/j.bmc.2015.01.029
19. Kareem HS, Ariffin A, Nordin N, Heidelberg T, Abdul-Aziz A, Kong KW, Yehye WA (2015) Correlation of antioxidant activities with theoretical studies for new hydrazone compounds bearing a 3,4,5-trimethoxy benzyl moiety. Eur J Med Chem 103:497–505. https://doi.org/10.1016/j.ejmech.2015.09.016
20. Kaya B, Özkay Y, Temel HE, Kaplancıklı ZA (2016) Synthesis and biological evaluation of novel piperazine containing hydrazone derivatives. J Chem 2016:1–7. https://doi.org/10.1155/2016/5878410
21. Lgaz H, Chung I-M, Albayati MR, Chaouiki A, Salghi R, Mohamed SK (2018) Improved corrosion resistance of mild steel in acidic solution by hydrazone derivatives: an experimental and computational study. Arab J Chem. https://doi.org/10.1016/j.arabjc.2018.08.004
22. Li Z, Wan H, Shi Y, Ouyang P (2004) Personal experience with four kinds of chemical structure drawing software: review on ChemDraw, ChemWindow, ISIS/Draw, and ChemSketch. J Chem Inf Comput Sci 44(5):1886–1890. https://doi.org/10.1021/ci049794h
23. Maltarollo VG, de Resende MF, Kronenberger T, Lino CI, Pinheiro Duarte Sampaio MC, da Rocha Pitta MG et al (2018) In vitro and in silico studies of antioxidant activity of 2-thiazolylhydrazone derivatives. J Mol Graphics Modell. https://doi.org/10.1016/j.jmgm.2018.10.007
24. Medina-Franco JL, Yoo J, Dueñas-González A (2015) DNA methyltransferase inhibitors for cancer therapy. Epigenet Technol Appl:265–290. https://doi.org/10.1016/b978-0-12-801080-8.00013-2
25. Melagraki G, Afantitis A, Sarimveis H, Koutentis PA, Kollias G, Igglessi-Markopoulou O (2009) Predictive QSAR workflow for the in silico identification and screening of novel HDAC inhibitors. Mol Divers 13(3):301–311. https://doi.org/10.1007/s11030-009-9115-2
26. Melagraki G, Afantitis A, Sarimveis H, Koutentis PA, Markopoulos J, Igglessi-Markopoulou O (2007) Optimization of biaryl piperidine and 4-amino-2-biarylurea MCH1 receptor antagonists using QSAR modeling, classification techniques and virtual screening. J Comput Aided Mol Des 21(5):251–267. https://doi.org/10.1007/s10822-007-9112-4
27. Mikulski D, Eder K, Molski M (2014) Quantum-chemical study on relationship between structure and antioxidant properties of hepatoprotective compounds occurring in cynara scolymus and silybum marianum. J Theor Comput Chem 13:1), 1–1),24. https://doi.org/10.1142/S0219633614500047
28. Mitra I, Saha A, Roy K (2011) Chemometric QSAR modeling and *in silico* design of antioxidant no donor phenols. Sci Pharm 79:31–58. https://doi.org/10.3797/scipharm.1011-02.
29. Najafi M, Mood KH, Zahedi M, Klein E (2011) DFT/B3LYP study of the substituent effect on the reaction enthalpies of the individual steps of single electron transfer-proton transfer and sequential proton loss electron transfer mechanisms of chroman derivatives antioxidant action. Comput Theor Chem 969:1–12. https://doi.org/10.1016/j.comptc.2011.05.006
30. Nenadis N, Tsimidou MZ (2012) Contribution of DFT computed molecular descriptors in the study of radical scavenging activity trend of natural hydroxybenzaldehydes and corresponding acids. Food Res Int 48:538–543. https://doi.org/10.1016/j.foodres.2012.05.014
31. Özbakır Işın D (2016) Theoretical study on the investigation of antioxidant properties of some hydroxyanthraquinones. Mol Phys 114(24):3578–3588. https://doi.org/10.1080/00268976.2016.1248514
32. Palepu NR, Richard Premkumar J, Verma AK, Bhattacharjee K, Joshi SR, Forbes S et al (2018) Antibacterial, in vitro antitumor activity and structural studies of rhodium and iridium complexes featuring the two positional isomers of pyridine carbaldehyde picolinic hydrazone ligand. Arab J Chem 11(5):714–728. https://doi.org/10.1016/j.arabjc.2015.10.011
33. Qurrat-ul-Ain, Ashiq U, Jamal RA, Saleem M, Mahroof-Tahir M (2017) Alpha-glucosidase and carbonic anhydrase inhibition studies of Pd (II)-hydrazide complexes. Arab J Chem 10(4):488–499. https://doi.org/10.1016/j.arabjc.2015.02.024
34. Rawat P, Singh RN, Niranjan P, Ranjan A, Holguín NRF (2017) Evaluation of antituberculosis activity and DFT study on dipyrromethane-derived hydrazone derivatives. J Mol Struct 1149:539–548. https://doi.org/10.1016/j.molstruc.2017.08.008
35. Renaud J-P, Moras D, Wurtz J-M (2007) Nuclear hormone receptors: insights for drug design from structure and modeling. Compr Med Chem II:725–747. https://doi.org/10.1016/b0-08-045044-x/00273-x
36. Rimarcik J, Lukes V, Klein E, Ilcin M (2010) Study of the solvent effect on the enthalpies of homolytic and heterolytic N–H bond cleavage in p-

phenylenediamine and tetracyano-p-phenylenediamine. J Mol Struct (THEOCHEM) 952:25–30. https://doi.org/10.1016/j.theochem.2010.04.002
37. Ruscic B (2015) Active thermochemical tables: sequential bond dissociation enthalpies of methane, ethane, and methanol and the related thermochemistry. J Phys Chem A 119(28):7810–7837. https://doi.org/10.1021/acs.jpca.5b01346
38. Sebeka AH, Osman AM, El Sayed IE, El-Bahanasawy M, Tantawy MA (2017) Synthesis and antiproliferative activity of novel neocryptolepine-hydrazides hybrids. J App Pharm Sci 7(10):009–015. https://doi.org/10.7324/JAPS.2017.71002
39. Shao Y, Molnar LF, Jung Y, Kussmann J, Ochsenfeld C, Brown ST et al (2006) Advances in methods and algorithms in modern quantum chemistry program package. Phys Chem Chem Phys 8(27):3172–3191. https://doi.org/10.1039/B517914A
40. Szeląg M, Mikulski D, Molski M (2011) Quantum-chemical investigation of the structure and the antioxidant properties of α-lipoic acid and its metabolites. J Mol Model 18(7):2907–2916. https://doi.org/10.1007/s00894-011-1306-y
41. Tariq QU, Malik S, Khan A, Naseer MM, Khan SU, Ashraf A, Ashraf M, Rafiq M, Mahmood K, Tahir MN, Shafiq Z (2019) Xanthenone-based hydrazones as potent α-glucosidase inhibitors: synthesis, solid state self-assembly and in silico studies. Bioorg Chem 84:372–383. https://doi.org/10.1016/j.bioorg.2018.11.053
42. Tissandier MD, Cowen KA, Feng WY, Gundlach E, Cohen MH, Earhart AD, Coe JV, Tuttle TRJ (1998) The proton's absolute aqueous enthalpy and Gibbs free energy of solvation from cluster-ion solvation data. J Phys Chem A 102(40):7787–7794
43. Vyas V (2008) Virtual screening: a fast tool for drug design. Sci Pharm 76(3): 333–360. https://doi.org/10.3797/scipharm.0803-03
44. Wang G, Xue Y, An L, Zheng Y, Dou Y, Zhang L, Liu Y (2015) Theoretical study on the structural and antioxidant properties of some recently synthesised 2,4,5-trimethoxy chalcones. Food Chem 171:89–97. https://doi.org/10.1016/j.foodchem.2014.08.106
45. Xue Y, Zheng Y, An L, Dou Y, Liu Y (2014) Density functional theory study of the structure–antioxidant activity of polyphenolic deoxybenzoins. Food Chem 151:198–206. https://doi.org/10.1016/j.foodchem.2013.11.064
46. Yap CW (2011) PaDEL-descriptor: an open source software to calculate molecular descriptors and fingerprints. J Comput Chem 32(7):1466–1474. https://doi.org/10.1002/jcc.21707
47. Zheng YZ, Deng G, Liang Q, Chen DF, Guo R, Lai RC (2017) Antioxidant activity of quercetin and its glucosides from propolis: a theoretical study. Sci Rep 7:7543. https://doi.org/10.1038/s41598-017-08024-8

Publisher's Note